Enormous improvement of mobility of 2D carrier gas using high-κ dielectric in SiGe quantum well

Rezvan Torkashvand[*] and Ghassem Ansaripour
Department of Physics, Faculty of Science, Bu-Ali Sina University, Hamedan, Iran

E-mail: gansaripour@basu.ac.ir

Abstract
Using different scattering mechanisms such as, surface roughness, alloy, charge impurity, strain, phonon scattering and regarding the effect of various dielectric constants, calculations of the carrier mobility in a strained SiGe quantum well on (001) Si are implemented. It is shown that the mobility of carriers inside the channel increases several times as a result of increasing the dielectric mismatch. At low temperatures, using a dielectric coating ($\kappa = 100$) the mobility rises from $1600 \, cm^2 \, V^{-1} \, s^{-1}$ to $12300 \, cm^2 \, V^{-1} \, s^{-1}$ which shows an increase of more than seven times, whereas at room temperature and same density the mobility increases from $760 \, cm^2 \, V^{-1} \, s^{-1}$ to $970 \, cm^2 \, V^{-1} \, s^{-1}$. In fact, increasing the dielectric constant weakens the screening effect and the attenuation of Coulomb potential. This mobility enhancement at low temperatures occurs for any carrier densities, but at high temperatures and low densities, the behavior is completely different. Failure to account for this dielectric mismatch causes incorrect results at high densities, and this becomes more obvious with increasing dielectric coefficient. The findings of this study emerge a comprehensive picture of the effect of dielectrics on charge transport in quantum well for low and room temperature at different carrier densities, as well as, help us to identify the optimal dielectric coating for the design and fabrication of the high mobility nanoscale transistors.

Keywords: mobility improvement, dielectric coating, scattering mechanisms, screening, quantum well

The continuous demand for smaller and faster devices has changed the geometry of devices from bulk to smaller dimensions, such as two-dimensional charged gases in modulation-doped quantum wells [1-3], graphene [4, 5], one-dimensional electron gases in nanotubes [6] and nanowires [7]. This is due to both the need for a large number of transistors on a chip and the increase in carrier mobility in a transistor for faster switching and lower power consumption. Hence, the physics of nanostructures (layers and wires) has become an active research area in the field of solid state devices. The dielectric mismatch between a nanoscale semiconductor material (relative dielectric constant ε_2 and the surrounding environment ε_1) can result in a number of peculiarities not present in their bulk and layered forms (such as epitaxially grown quantum wells and superlattices). In this work, we propose a novel technique for improving the electron mobility in such bottom-up 2D semiconductor nanostructures by showing that the dielectric environment has a profound effect on electron transport which do not require the stringent lattice-matching requirements placed by epitaxy.

The effect of the dielectric environment on the charge transport properties of nanostructures has not been studied as extensively as its effect on optical properties [8].

However, some studies have investigated the effect of the dielectric environment on Coulomb scattering and surface roughness in two dimensions [9-11] and one dimension [12,13]. These studies have shown that neglecting dielectric mismatch leads to inaccurate scattering rates, which becomes less important in one dimension and at higher dielectric constants but more crucial at lower constants.

Additionally, it has been predicted that the Coulomb potential in both two and one dimensions is significantly affected by the dielectric environment [14,15], a fact later confirmed by experimental results. Furthermore, another study [16] examined the effect of dielectric mismatch in one dimension for various scattering mechanisms but excluded the limiting cases of surface roughness and alloy scattering. Another work [17] only considered the impact of dielectric mismatch on the combined effect of Coulomb and phonon scattering. Similarly, the influence of dielectric coating on a graphene layer has only been explored for surface roughness and Coulomb scattering [18,19].

Scattering mechanisms mediated by long-range Coulomb interactions, such as charged impurities, polar optical phonons, and piezoelectric acoustic phonons, can be effectively screened by free carriers.
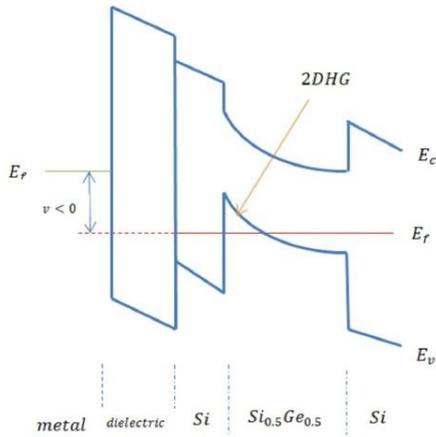
Figure 1. Energy band diagram for SiGe and formation of two-dimensional hole gas under an applied negative gate bias.
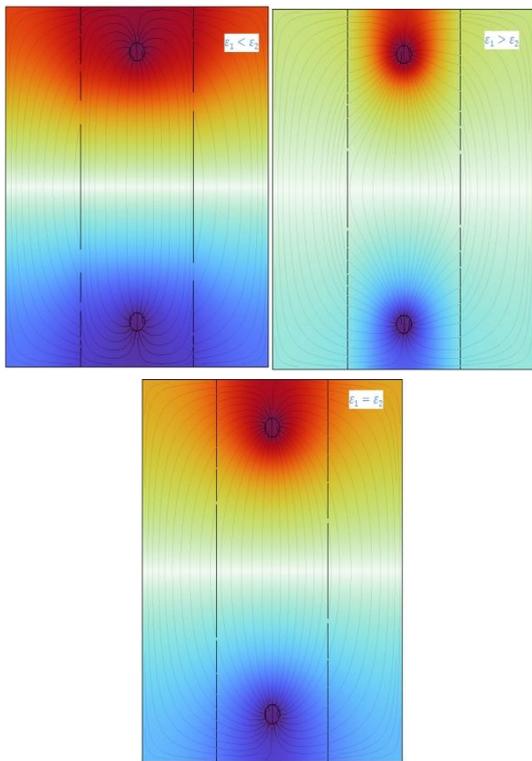
Figure 2. Variation of field lines and Coulomb potential resulting from the dielectric difference inside and outside the dielectric layer. ε_1 represents the dielectric constant of the cover, and ε_2 is the dielectric constant of the channel. As the dielectric of the environment increases from 1 to 100, the potential decreases.

Neglecting the dielectric mismatch in the screening function leads to inaccurate results. However, free carriers may not respond to rapidly varying scattering potentials that arise from short-range interactions [17].

An alloy of silicon and germanium, two well-known semiconductor elements, can form the basis of very high-speed transistors. Previously, different mobilities for $Si_{0.8}Ge_{0.2}$ channel without dielectric mismatch have been calculated [20]. This paper investigates the mobility of carriers considering dielectric mismatch in a heterojunction metal oxide semiconductor (MOSFET) structure with SiGe channel. To this end, the effect of

various scatterings has been considered at very low temperatures as well as room temperature. In this work the potential well considered here is a triangular because it is more realistic, and five different scatterings have been regarded, but in [9,12], a square potential well and only with two different scatterings have been considered. The availability of high-quality insulating materials with a very wide range of relative dielectric constants ($1 < \varepsilon < 300$) shows that the proposed mobility improvement technique can be implemented with current technology. In this study, we have studied different scattering mechanisms in the first section, carrier mobility at low temperature in the second section, and carrier mobility at room temperature in the last section.

To significantly improve the performance of devices and understand the transport in Si_xGe_{1-x} systems, investigating fundamental scatterings [21-23] is essential. This article reviews these scatterings, including surface roughness, alloy, strain, charge impurity, and phonon. we ignore phonon scattering (optical and acoustic) at low temperatures [24]. Determining the exact contribution of each of these mechanisms remains challenging, both experimentally and theoretically [25]. Figure 1 depicts the energy band diagram for the SiGe channel in a MOSFET. With a negative gate voltage and the rejection of electrons from the oxide surface, the energy bands bend upwards, causing carriers to accumulate near the surface and form a two-dimensional gas.

In figure 2, we schematically depict the influence of dielectric coating on the Coulomb potential, a crucial scattering mechanism at low temperatures. The figure demonstrates that if the dielectric constant of the coating is higher than that of the channel layer (figure on the right), the Coulomb potential inside the layer decreases, causing the field lines inside the channel to move away. This results in an increased mobility. Conversely, when the dielectric constant of the coating is lower than that of the layer (figure on the left), the potential inside the channel increases, leading to a decrease in mobility as the field lines inside the channel approach. For triangular quantum wells, the lowest energy band employs the Fang-Howard wave function [26]

$$\chi_1(Z) = \sqrt{\frac{b^3}{2}} \, Z \tag{1}$$

$$b = \left[\frac{12 \, m_z \, e^2}{\hbar \, \varepsilon_l} \left(N_d + \frac{11}{32} \, N_s \right) \right]^{1/3} \tag{2}$$

b having the reciprocal unit of length, serves as the parameter representing the thickness of the potential well. where ε_l is the dielectric constant of the host lattice, m_z is the effective mass in the growth direction, N_s is he carrier concentration of carrier, N_d is the depletion charge density, e is the elementary charge. The scattering rate and dielectric function are also expressed in the following manner

$$\frac{1}{\tau(E)} = \frac{1}{2\pi E} \int_0^{2k} \frac{q^2 \langle |U(q)|^2 \rangle}{\varepsilon(q)^2 \sqrt{(2k)^2 - (q)^2}} dq \tag{3}$$

where $U(q)$ represents the random scattering potential. The primary contribution of this integral is notable when $q \cong 2k_F$. The screened potential $U_{scr}(q, \omega)$, is lowered from the unscreened potential $U_{uns}(q, \omega)$, by dielectric function $\varepsilon(q, \omega)$

$$U_{scr}(q, \omega) = \frac{U_{uns}(q,\omega)}{\varepsilon(q,\omega)} \tag{4}$$

$$\varepsilon(q, \omega) = 1 - U_q \sum_q \frac{f_{k+q} - f_k}{(E_{k+q} - E_k) + \hbar\omega} \tag{5}$$

where E_k is the energy level of the carrier. At a finite temperature T, the static screening by a free 2D carrier gas is described by Lindhard function

$$\mathcal{E}_q(T) = 1 + \frac{q_s}{q} F(q)\Pi(q, T)\left(1 - G_H(q)\right) \tag{6}$$

q_s is the reciprocal screening length in two dimensions, $G_H(q)$ denotes the Hubbard correction of the local field. In this context, $G(2k_F) = 0.447$ [27], and $\Pi(q, T)$ is assessed as the polarizability. It's worth noting that for the purposes of our discussion, we have disregarded its temperature dependence. However, in a separate study [28], the temperature dependence of $\Pi(q, T)$ has been explored in both two and three dimensions

$$q_s = \frac{e^2 m^*}{2\pi\hbar^2 \varepsilon_0 \mathcal{E}_s} \tag{7}$$

where $\mathcal{E}_s$ is the dielectric constant of the semiconductor, $\mathcal{E}_0$ vacuum permittivity, e is the elementary charge, m^* is hole effective mass. Additionally, $F(q)$ represents the form factor, and its calculation incorporates considerations for dielectric mismatch [29]

$$F(q) = \frac{1}{2}\left(1 + \frac{\varepsilon_1}{\varepsilon_2}\right)\left[1 + \frac{9}{8}\left(\frac{q}{b}\right) + \frac{3}{8}\left(\frac{q}{b}\right)^2\right]\left(1 + \frac{q}{b}\right)^{-3} + \frac{1}{2}\left(1 - \frac{\varepsilon_1}{\varepsilon_2}\right)\left(1 + \frac{q}{b}\right)^{-6} \tag{8}$$

In this context, ε_2 represents the dielectric constant of the channel, and ε_1 is the dielectric constant of the cover. When the scatterings are considered independent, the rates combine, and this summation is computed for elastic scattering using Matheissen's law [30]

$$\tau(E) = \left(\sum_i \tau_i(E)^{-1}\right)^{-1} \tag{9}$$

In general, mobility is calculated as follows:

$$\mu = \frac{e}{4\pi\hbar^2 N_s k_B T} \int_0^\infty \frac{E\tau(E)dE}{\cosh^2[(E - \xi)/2k_B T]} \tag{10}$$

Where k_B is the Boltzmann constant, At low temperatures, mobility is determined through the relationship $\mu = e\tau(E_F)/m^*$ [31]. Taking into account the influence of dielectric mismatch in the dielectric function, we have computed various scattering contributions.

Any sudden change in the surface induces a variation in the thickness of the quantum well, consequently impacting the specific energy states. When these irregularities span the entire interface, the disruption of the energy levels establishes an effective electric potential for carriers traversing along the channel. In theory, surface roughness is modeled using two parameters: the correlation length (Λ) and the roughness domain height (Δ). A rougher surface corresponds to a smaller Λ and a larger Δ. The scattering potential is expressed as follows

$$\langle|U(q)|^2\rangle = \pi(\Delta\Lambda)^2 q_s^2 E_F^2\left(1 + \frac{2N_{Dep}}{N_s}\right)^2 e^{-q^2\Lambda^2/4} \tag{11}$$

where E_F is the Fermi energy. Variations in the values of Λ result in different scattering outcomes. There are three distinct modes for this type of scattering: $k_F\Lambda \gg 1$, $2: k_F\Lambda \ll 1$, $3: k_F\Lambda \cong 1$, where k_F is the Fermi wave vector. In the third mode, mobility attains its maximum value [27].

Carriers experience scattering due to the inherently random nature of the alloy, constituting a significant limitation that persists unless the alloy is grown systematically. Typically, screening effects in alloy scattering are neglected due to their short range [32]. The mobility of carriers in alloy scattering in two dimensions was initially explored by V. Venkataraman et al. for electrons in a SiGe quantum well [33].

$$\langle|U(q)|^2\rangle = x(1 - x)\Omega_0 \delta E^2 \frac{3b}{16} \tag{12}$$

Here, $\Omega_0 = \frac{a_0^3}{8}$, a_0 is the lattice constant of the alloy. and δE represents the strength of the scattering potential [34]. There is a lack of consensus regarding the precise value of the alloy potential [35]; however, in this context, $\delta E \sim 0.6$ eV.

Extensive efforts have been devoted to modeling charge impurity scattering [36-38], and in this study, we employed the analysis proposed by [39] for our calculations. The increase in impurity concentration corresponds to an increase in scattering. Regarding charge impurities located within the semiconductor, the Coulomb potential is derived as follows

$$\langle|U(q)|^2\rangle = N_i\left(\frac{e^2}{2E_l q^2}\right)^2 F_i(q) \tag{13}$$

where N_i is the impurity density

$$F_i(q) = \left(\frac{b}{q+b}\right)^6 \tag{14}$$

Here, $F_i(q)$ represents the impurity scattering form factor [40].

In the context of a thin quantum well channel, enveloped by strain-free barrier layers, strain relaxation takes place in the channel during growth to minimize the overall energy of the system. Two forms of strain relaxants exist: elastic, contributing to surface roughness, and plastic, leading to undesirable dislocations in a film. Both types of relaxation induce strain alterations in the channel layer. These alterations serve as a significant potential source of electron scattering, thereby potentially limiting the mobility of devices. In this study, we explore the scattering arising from strain changes due to roughness [41]. This type of scattering enhances carrier mobility by alleviating degeneracy in the energy bands and reducing the effective mass [42]

$$\langle|U(q)|^2\rangle = \frac{\pi\Lambda^2\Delta^2\Xi^2 f^2}{4}\frac{(1+\nu)^2}{(1-\nu)^2}F_i(q)\exp(-q^2\Lambda^2/4) \tag{15}$$

Where $f = 0.01$ is the lattice mismatch factor, Ξ is the deformation potential, $\nu = 0.28$ is Poisson's ratio[40].

The coupling of carrier transport with acoustic phonons can occur through deformation potentials or piezoelectric components. Since the acoustic phonon branch has both longitudinal and transverse modes, ideally both should be considered when determining the scattering rate. However, transverse modes are weaker than longitudinal modes when it comes to scattering via the deformation potential. In the case of piezoelectric coupling, both longitudinal and transverse modes must be taken into account. Nevertheless, it has been demonstrated that the piezoelectric component of acoustic phonon scattering is weaker than the deformation potential scattering and may be neglected. Therefore, in this analysis, only scattering by the longitudinal mode of acoustic phonons is considered [43]

$$\langle|U(q)|^2\rangle = \frac{3E_D^2 k_B T b}{16\rho u_l^2} \tag{16}$$
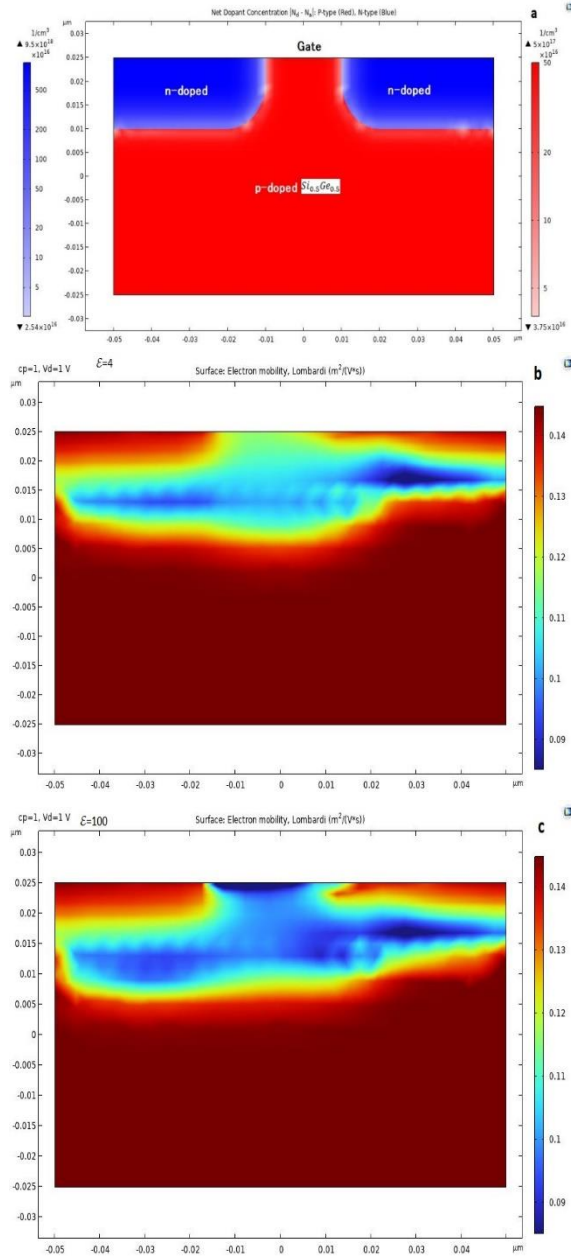
Figure 3: Lombardi mobility model for $Si_{0.5}Ge_{0.5}$ MOSFET. a) Geometric characteristics of MOSFET. b) Lombardi mobility for dielectric $\varepsilon = 4$ c) Lombardi mobility for $\varepsilon = 100$.
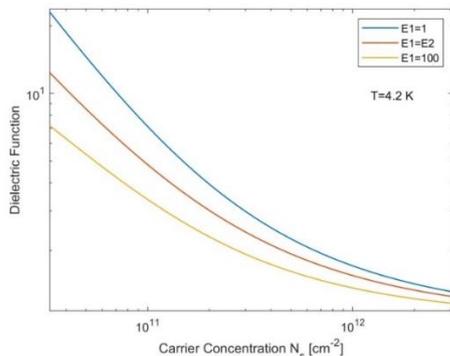
Figure 4. Dielectric function versus carrier density for different dielectrics. This shows that the effect of dielectric mismatch on screening is substantial if the density of carrier is large.

Where ρ is the density of the crystal, u_l is the longitudinal acoustic phonon velocity, E_D is the deformation potential constant.

Below example demonstrates how to use the Lombardi surface scattering model for the electron mobility in a simple MOSFET with comsol Simulator. Surface acoustic phonons and surface roughness have an important effect on the carrier mobility, especially in the thin inversion layer under the gate in MOSFETs. The Lombardi surface mobility model adds surface scattering resulting from these effects to an existing mobility model using Matthiessen's rule. The mobility model is based on the equations presented in [44,45]. The model represents a 2D MOSFET where the n-doped drain and source contacts are located at the top right and top left of the geometry, respectively; see figure 3a. The gate is positioned above the p-doped $Si_{0.5}Ge_{0.5}$ section which is located at the center of the device. With the simulation, we came to the conclusion that increasing the dielectric constant of the gate decreases the surface mobility Contains phonon and surface roughness in the channel.

As discussed below with the increase of dielectric constant, all type of mobilities decrease except Coulombic mobilities (see figure 3b and 3c). This is a confirmation to advance our goals to be able to examine different mobility models at different temperatures for different channels.

At low temperatures, carriers exhibit high degeneracy and behave akin to a two-dimensional Fermi gas. The dielectric environment surrounding the semiconductor significantly influences the mobility of carriers within the semiconductor. The dominant scattering mechanisms under these conditions are surface roughness scattering and charged impurity scattering, both of which display a pronounced dependence on the dielectric mismatch between the cover and the channel. The relevant parameters utilized in this study are listed in Table 1.

In figure 4, the curve illustrates changes in the dielectric function concerning carrier density for various dielectrics. This curve indicates a decrease in the screening effect and the elimination of the dielectric mismatch effect with an increase in carrier density. In one dimension, the dielectric function also rises with an increase in carrier density [13]. The impact of the difference in the dielectric constant of the environment is such that a higher dielectric constant correlates with reduced scattering [46]. Reduced screening implies increased dispersion.

In a related study [47], accounting for the screening effect, various mobilities were investigated for $Si_{0.5}Ge_{0.5}$, where impurity charge scattering dominates at low densities. An increase in in N_s or N_{dep} causes an increase in surface roughness scattering, so surface roughness scattering becomes dominant at high densities. The presence of both surface roughness and impurity charge scattering leads to a peak in the mobility curve. The dielectric environment surrounding the semiconductor impacts the mobility of the carriers within it.

In figure 5-a, the mobility in the $Si_{0.5}Ge_{0.5}$ channel for different environments is illustrated, indicating a significant increase in mobility with varying dielectric coatings. With a constant dielectric constant of $k = 100$,

the mobility reaches approximately $12000\ \mathrm{cm^2V^{-1}s^{-1}}$. In contrast, with a vacuum coating, the mobility is around $600\ \mathrm{cm^2V^{-1}s^{-1}}$. This indicates that altering the dielectric constant of the environment can result in a mobility increase of up to 20 times.

Unlike Figure 4, in this case, at low densities, the influence of dielectric mismatch on scattering diminishes. This is attributed to the significant decrease in the charge impurity potential with a larger dielectric constant, indicating higher sensitivity to dielectric differences than the screening function. The reduction in charge impurity potential, in fact, has a more pronounced effect on mobility than the decrease in screening. The thickness of the channel, denoted as Z, is related to the carrier density in the triangular quantum well, with $Z = 3/b$. In part b, calculations for carriers in the potential well $Si_{0.5}Ge_{0.5}$ reveal that surface roughness scattering is limiting for well widths $z < 90$ Å at low temperatures with a vacuum cover. For greater thicknesses, charge impurity scattering becomes the limiting factor, and in this specific thickness range, the mobility is maximized. With an increase in dielectric constant, the thickness at which mobility is maximum also increases. The figure presented includes only surface roughness and impurity charge scattering as they are the limiting factors, omitting the other scattering mechanisms for ease of comparison. In figure 6, the mobilities of Si and $Si_{0.5}Ge_{0.5}$ for different dielectrics are compared, show casing the consistently lower mobility of Si. In the Si channel, where there is no alloy scattering, surface roughness scattering is the limiting factor.

The investigation of mobility at room temperature for $Si_{0.5}Ge_{0.5}$ and Si coatings, considering the screening effect, has been conducted previously. However, these studies did not account for the impact of different dielectrics [48]. In this scenario, phonon and alloy mobilities contribute the most, but as the Ge concentration decreases at lower temperatures, surface roughness scattering becomes dominant. The maximum mobility value at a temperature of approximately $60\ \mathrm{K}$ is about $4800\ \mathrm{cm^2V^{-1}s^{-1}}$. Additionally, with an increase in the concentration of germanium, the temperature at which phonon scattering becomes dominant also increases.

In figure 7a, we explored the impact of different dielectrics on carrier mobility concerning temperature. As the temperature rises, the screening effect weakens, and a significant increase in mobility is observed with a dielectric coating featuring a constant of 100 compared to the Si coating.

For coatings with a constant close to that of the dielectric constant of the channel, a peak appears in the curve near the Fermi temperature due to the influence of surface roughness and alloy scattering. However, at high constants, only alloy scattering is dominant, and the effect of surface roughness becomes negligible, leading to the disappearance of the curve peak. At room temperatures, even at high carrier densities, phonon scattering takes precedence, and its weak dependence on dielectric changes is only through the dielectric function. Consequently, it can be inferred that the screening effect becomes very weak at higher temperatures.
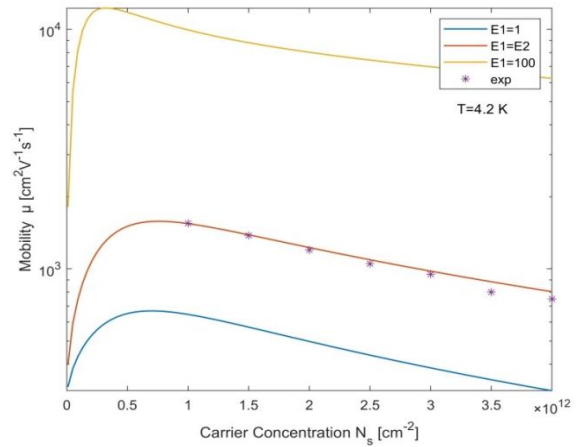

(a)
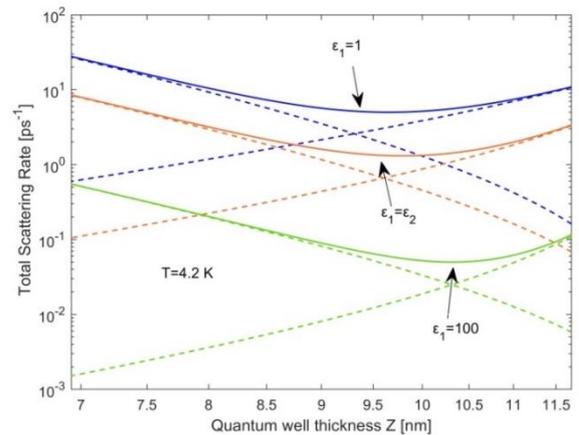
(B)

Figure 5. a) Carrier mobility at low temperature in the $Si_{0.5}Ge_{0.5}$ channel for different dielectrics compared to N_s. Theory (-) and experimental results (*) [47]. A large increase in mobility is expected for thin semiconductor layer coated by dielectric with high constant b) carrier scattering at low temperature $Si_{0.5}Ge_{0.5}$ for different dielectrics relative to the channel thickness. Two important scatters including charge impurity surface roughness, and the total scatter are shown.
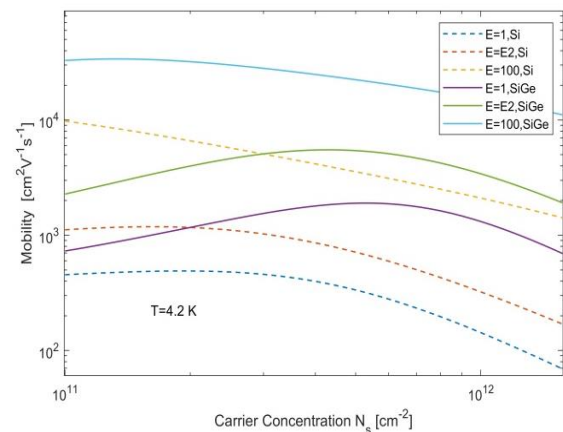
Figure 6. Carrier mobility at low temperature of $Si_{0.5}Ge_{0.5}$ and Si channels for different dielectrics respect to N_s. The mobility of Si is always lower than $Si_{0.5}Ge_{0.5}$
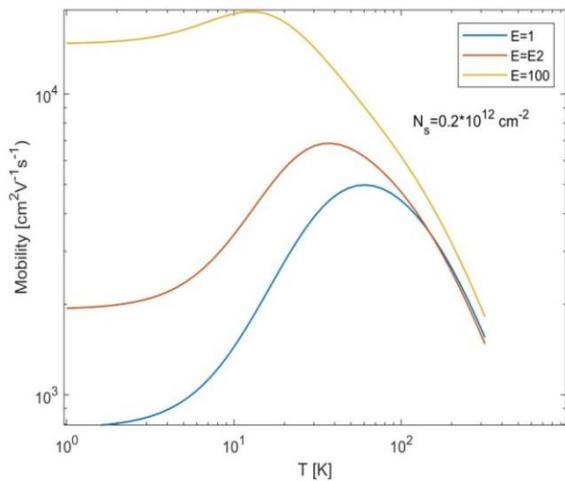
(a)
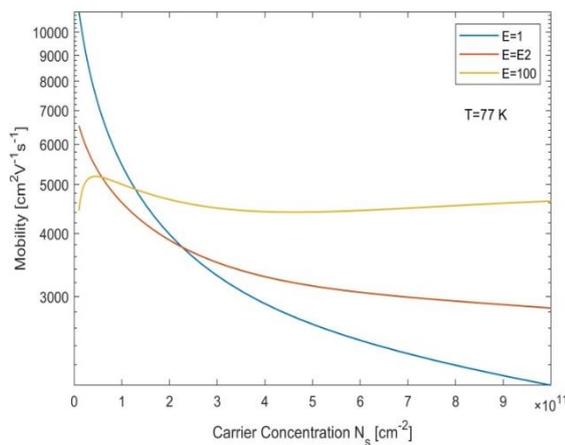
(b)

Figure 7. a) Carrier mobility for $Si_{0.5}Ge_{0.5}$ channel versus temperature in different dielectrics $N_S = 10^{12} \ cm^{-2}$. carrier mobility inside a thin membrane can be significantly enhanced even at room temperature b) Carrier mobility for $Si_{0.5}Ge_{0.5}$ channel versus carrier density in different dielectrics at temperature $T = 300$ K. The effect of dielectric mismatch is not constant.

At high densities, alloy mobility consistently serves as the limiting factor. Therefore, at low densities (in contrast to the mobility diagram at low temperature), the mobility curve in figure 7b exhibits changes where mobility decreases at low densities with an increasing dielectric constant. In other words, a vacuum coating performs better than any other coating. However, around $N_S = 0.2 \times 10^{12} \ cm^{-2}$, coatings with higher coefficients outperform silicon constant and exhibit higher mobility. With an increase in germanium concentration, this effect diminishes and for dielectric coatings with a constant greater than that of the channel by carrier density increase leads to an enhancement in mobility. At a temperature of 77 K, there is a significant increase in mobility. In figure 8, an examination of mobility changes at room temperature and low temperature concerning the dielectric constant of the environment is presented for two cases: with and without considering dielectric mismatch in the screening function.
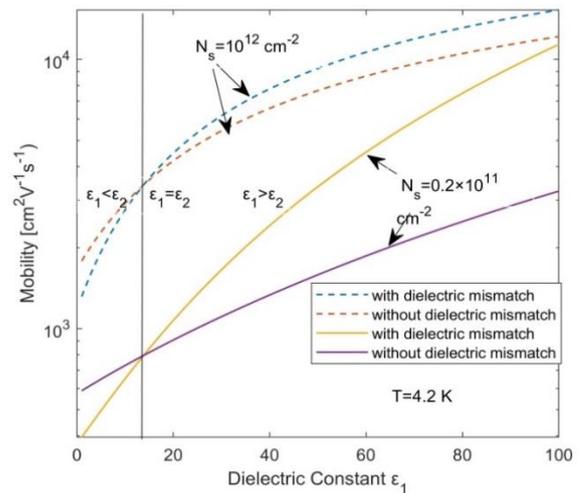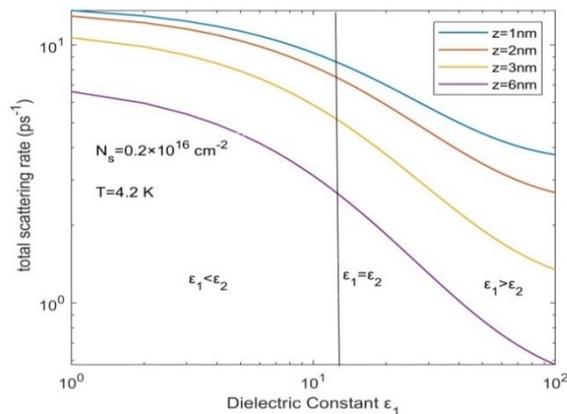

(a)
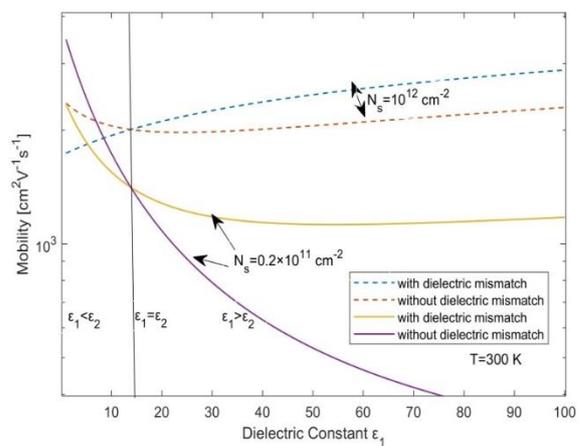
(b)

Figure 8. In dielectric constants higher than the channel and at all temperatures, calculating the dielectric mismatch increases the mobility a) The total mobility at low temperature compared to the dielectric constant of the environment for $N_s = 10^{12} \ m^{-2}$ (dashed line) and $N_s = 0.2 \times 10^{11} \ cm^{-2}$ (solid line) b) The total mobility at a temperature of 300 K with respect to the dielectric constant of the environment for $N_s = 10^{12} \ cm^{-2}$ (dashed line) and $N_s = 0.2 \times 10^{11} cm^{-2}$ (solid line).

The conclusion drawn is that it is more critical to take into account dielectric mismatch in the screening function at constants higher than the surrounding constant. Failing to calculate it may lead to incorrect results.
In the previous works on one dimension, the consideration was predominantly on the impact of dielectric mismatch on charge impurity potential. However, it is essential to recognize that surface roughness at low temperatures and phonon scattering at higher temperatures are also decisive factors. Here, we have comprehensively reviewed all the scattering mechanisms that may influence the mobility of carriers. At higher densities, the dielectric function becomes much more sensitive to dielectric mismatch. This heightened sensitivity is due to the strengthened impact of Coulomb scattering and surface roughness with increasing carrier density. In this type of scattering, dielectric difference not only affects the screening function but also influences the scattering potential.

Table 1. Parameters used in the article

correlation length [48,49]	average height of roughness [48,49]	effective mass [30]	effective mass in the growth direction [30]	charge impurity density [48]	depletion charge density	alloy potential [48]
Λ	Δ	m^*	m_z	N_i	N_d	δE
3.5 nm	0.58 nm	$0.22 m_0$	$0.25 m_0$	$1.5 \times 10^{11} \text{cm}^{-2}$	10^{11}cm^{-2}	0.6 eV

Figure 9. The total scattering rate in terms of the dielectric

An increase in the dielectric constant results in an increase in mobility. In this analysis, the effect of temperature on the dielectric function has been neglected, and only the impact of temperature on mobility has been calculated. figure 9 illustrates the changes in scattering for different thicknesses of the $Si_{0.5}Ge_{0.5}$ channel. In smaller thicknesses, the rate of dispersion changes is less sensitive to the dielectric coating. However, for dielectrics with a constant higher than that of the channel, the dispersion changes are more pronounced. In smaller thicknesses and constants lower than the dielectric constant of the channel, the impact of dielectric difference can be disregarded. Also, at low densities, the effect of dielectric difference can be neglected for constants lower than the channel constant. This is because at low densities, the penetration of the wave function of the carriers to the boundaries is less, resulting in a diminished scattering effect of surface roughness. Additionally, the smaller the thickness of the channel, the more carriers will be concentrated near the boundaries, leading to increased surface roughness scattering and a subsequent decrease in carrier mobility. constant of the coating for different channel thicknesses $Si_{0.5}Ge_{0.5}$ in $N_s = 0.2 \times 10^{16} \text{ m}^{-2}$. Increasing the channel thickness reduces the scattering rate.

Conclusion

The enhancement of carrier mobility in two-dimensional structures can be substantial through the application of dielectric coatings. For low carrier densities at room temperature, optimal improvements in carrier mobility are achieved with dielectrics possessing lower dielectric constants. Conversely, at low temperatures, regardless of density, increased dielectric constants lead to improved mobility. Our results indicate that considering dielectric mismatch in the screening function can enhance mobility by nearly eight times at low temperatures. Although this increase is less pronounced at room temperature. Neglecting dielectric mismatch in the screening function results in inaccurate outcomes. The larger the dielectric coating constant, the greater the divergence between the results obtained by considering and not considering the dielectric mismatch. In essence, the importance of calculating dielectric mismatch is more significant at higher constants. Furthermore, the impact of dielectric mismatch on carrier mobility is significantly less at low densities compared to high densities. The high sensitivity of carrier mobility in such layers to the dielectric environment holds potential for sensor applications, providing an attractive avenue for enhancing the performance of nanostructured electronic devices.

References

1. L Tao, E Cinquanta, D Chiappe, C Grazianetti, M Fanciulli, M Dubey, and A Molle, Nature Nanotechnology **10** (2015) 227.
2. K H Aharonyan, E M Kazaryan, M Bazzan, and E P Kokanyan, Physica B **695** (2024) 416535.
3. D K Efetov and P Kim, Physical Review Letters **105** (2013) 256805.
4. M Xu, T Liang, M Shi, and H Chen, Chemical Reviews **113** (2013) 3766.
5. S Das Sarma, S Adam, E Hwang, and E Rossi, Reviews of Modern Physics **83** (2011) 407.
6. J C Charlier, X Blasé, and S Roche, Reviews of Modern Physics **79** (2007) 677.
7. C M Lieber, MRS Bulletin **28** (2003) 486.
8. D Zanato, S Gokden, N Balkan, B K Ridley, and W J Schaff, Semiconductor Science and Technology **19** (2004) 427.
9. D Jena and A Konar, Physical Review Letters **98** (2007) 136805.
10. A Konar, M Bajaj, R K Pandey, and K V R M Murali, Journal of Applied Physics **114** (2013) 113707.
11. N Ma and D Jena, Physical Review X **4** (2014) 011043.
12. D Jena and A Konar, Journal of Applied Physics **102** (2007) 123705.
13. A Konar, T Fang and D Jena, Physical Review B **84** (2011) 085422.

14.   L V Keldysh, JETP Letters **29** (1979) 658.
15.   L V Keldysh, Physica Status Solidi (a) **164** (1997) 3.
16.   G Ansaripour and B Shayeghy, Optik **127** (2016) 9673.
17.   H Sakaki, T Noda, K Hirakawa, M Tanaka and T Matsusue, Applied Physics Letters 51 (1987) 1934.
18.   A Konar, T Fang and D Jena, Physical Review B **82** (2010) 115452.
19.   A K M Newaz, Y S Puzyrev, B Wang, S T Pantelides and K Bolotin, Nature Communications **3** (2012) 734.
20.   G Ansaripour, Thin Solid Films **518** (2010) 5599.
21.   G Ansaripour, Thin Solid Films **517** (2009) 6105.
22.   G Ansaripour, G Braithwaite, S Agan, E H C Parker and T E Whall, Microelectronic Engineering **51** (2000) 541.
23.   M Myronov, Y Shiraki, T Mouri and K M Itoh, Thin Solid Films **517** (2008) 359.
24.   J H Davies, The Physics of Low-Dimensional Semiconductors (1998).
25.   W Zhang and Z Huang, Nano Research **7** (2014) 1731.
26.   M G Arashti and M A Sadeghzadeh, Vacuum **93** (2013) 1.
27.   C J Emeleus, T E Whall, D W Smith, R A Kubiak, E H C Parker and M J Kearney, Journal of Applied Physics **73** (1993) 3852.
28.   S D Sarma and E H Hwang, Scientific Reports **5** (2015) 16655.
29.   A Gold and V T Dolgopolov, Physical Review B **33** (1986) 1076.
30.   C Y Huang, J J M Law, H Lu, D Jena, M J W Rodwell and A C Gossard, Journal of Applied Physics **115** (2014) 123711.
31.   D R Leadley, M J Kearney, A I Horrell, H Fischer, L Risch, E H C Parker and T E Whall, Semiconductor Science and Technology **17** (2002) 708.
32.   J M Hinckley and J Singh, Physical Review B **41** (1990) 2912.
33.   V Venkataraman, C W Liu and J C Sturm, Applied Physics Letters **63** (1993) 20.
34.   A Rahmani, M A Sadeghzadeh and R Khordad, Superlattices and Microstructures **83** (2015) 271.
35.   G Ansaripour, G Braithwaite, M Myronov, O A Mironov, E H C Parker and T E Whall, Applied Physics Letters **76** (2000) 1140.
36.   S B Lisesivdin, A Yildiz, N Balkan, M Kasap, S Ozcelik and E Ozbay, Journal of Applied Physics **108** (2010) 013712.
37.   S Gokden, Physica E: Low-dimensional Systems and Nanostructures **23** (2004) 19.
38.   V M Polyakov and F Schwierz, Journal of Applied Physics **101** (2007) 033703.
39.   A Gold, Physical Review B **35** (1987) 723.
40.   R J P Lander, M J Kearney, A I Horrell, E H C Parker, P J Phillips and T E Whall, Semiconductor Science and Technology **12** (1997) 1064.
41.   R M Feenstra and M A Lutz, Journal of Applied Physics **78** (1995) 6091.
42.   S H Huang, T M Lu, S C Lu, C H Lee, C W Liu and D C Tsui, Applied Physics Letters **101** (2012) 042111.
43.   W Knap, S Contreras, H Alause, C Skierbiszewski, J Camassel, M Dyakonov, J L Robert, J Yang, Q Chen, M A Khan, M L Sadowski, S Huant, F H Yang, M Goian, J Leotin and M S Shur, Applied Physics Letters **70** (1997) 2123.
44.   C Lombardi, S Manzini, A Saporito and M Vanzi, IEEE Transactions on Computer-Aided Design of Integrated Circuits and Systems **7** (1988) 1164.
45.   M N Darwish, J L Lentz, M R Pinto, P M Zeitzoff, T J Krutsick and H H Vuong, IEEE Transactions on Electron Devices **44** (1997) 1529.
46.   V K Sangwan and M C Hersam, Annual Review of Physical Chemistry **69** (2018) 299.
47.   D R Leadley, M J Kearney, A I Horrell, H Fischer, L Risch, E H C Parker and T E Whall, Semiconductor Science and Technology **17** (2002) 708.
48.   M J Kearney and A I Horrell, Semiconductor Science and Technology **13** (1998) 174.
49.   M A Sadeghzadeh, A I Horrell, O A Mironov, E H C Parker, T E Whall and M J Kearney, Applied Physics Letters **76** (2000) 2568.